PCCP

# Ultraviolet charge-transfer-to-solvent spectroscopy of halide and hydroxide ions in subcritical and supercritical water



| | |
|---|---|
| Journal: | *Physical Chemistry Chemical Physics* |
| Manuscript ID | CP-ART-07-2019-003805.R1 |
| Article Type: | Paper |
| Date Submitted by the Author: | 08-Oct-2019 |
| Complete List of Authors: | Marin, Timothy; Benedictine University, Physical Sciences<br>Janik, Ireneusz; University of Notre Dame, Radiation Laboratory<br>Bartels, D; University of Notre Dame, Notre Dame Radiation Laboratory |
| | |

ARTICLE

# Ultraviolet charge-transfer-to-solvent spectroscopy of halide and hydroxide ions in subcritical and supercritical water

Timothy W. Marin,*[a, b] Ireneusz Janik [b] and David M. Bartels [b]

Received 00th January 20xx,
Accepted 00th January 20xx

DOI: 10.1039/x0xx00000x

The temperature dependence of the vacuum ultraviolet charge-transfer-to-solvent (CTTS) absorption spectra of aqueous halide and hydroxide ions was measured for the first time up to 380 °C in subcritical and supercritical water. With increasing temperature, absorption spectra are observed to broaden and redshift, much in agreement with previous measurements below 100 °C. These changes are discussed alongside classic cavity models of the solvated species, which tie in the configuration of the adjoining polarized medium and its critical role in light absorption for electronic transitions. The data seemingly confirm the validity of the "diffuse" model pioneered by Platzman and Franck and later revised by Stein and Treinin, which has largely gone untested for nearly 60 years due to lack of experimental data in this extended temperature range. A gradual increase in anion cavity size is inferred as a function of increasing temperature while the enthalpy and entropy of hydration are largely unaffected. The changes in solvation properties are considered in the context of recent studies of the ultraviolet spectroscopy of subcritical and supercritical water and historic studies of the CTTS absorption. The "diffuse" polarizable continuum model succeeds in describing the absorption due to lack of well-defined ion hydration shells for these ions. CTTS spectra for iodide in supercritical water show no energy shift as a function of pressure/density, suggesting dielectric saturation of the $I^-$ anion by the adjacent $H_2O$ molecules at all experimental pressures/densities.

## 1. Introduction

Simple inorganic anions such as $OH^-$, $NO_3^-$, $SO_4^{2-}$, and halides do not possess bound excited electronic states in the gas phase. Photoabsorption of deep/vacuum ultraviolet radiation leads to electron detachment, giving a structureless spectrum. However, in high-polarity solvents an intense, broad ultraviolet absorption arises, indicating that bound electronic states indeed exist.[1] Since the solvents lack the unoccupied orbitals necessary to stabilize the excess electron, these excited states are supported by many solvent molecules as a collective. Because of this means of the solvent supporting the excited states, they are dubbed charge-transfer-to-solvent (CTTS) states.[2] These states are markedly sensitive to the surrounding local solvent environment, making CTTS spectroscopy an excellent tool for exploring single ion solvation. Historically CTTS spectra have garnered significant interest in that they provide direct insight into the simplest of electron-transfer processes.[1]

A considerable body of work in the mid-20th century focused on the temperature, pressure, and solvent dependence of CTTS bands, and simple theoretical models were developed to describe them. This work was comprehensively reviewed by Blandamer and Fox.[1] In all of the early theoretical treatments, the molecular structure of the solvent shells surrounding the solute was largely ignored in favor of an averaged solvent continuum. In the mid-1950s, Platzman and Franck first presented a fundamental CTTS model that became the basis for later treatments.[3] The solvent is treated as a dielectric continuum with static and optical dielectric constants $\varepsilon_s$ and $\varepsilon_{op}$, respectively. The photoexcited electron is electrostatically trapped by the potential field induced through polarization of the medium by the ground-state anion. With simple Landau theory of continuous media employed, the CTTS states are considered to be hydrogenic with an effective charge of $-e\left[1/\varepsilon_{op} - 1/\varepsilon_s\right]$, giving a potential field

$$V(r) = -\frac{e}{r}\left(\frac{1}{\varepsilon_{op}} - \frac{1}{\varepsilon_s}\right) \qquad (1)$$

Here $e$ and $r$ are the electronic charge and the distance from the anion center. The energy associated with the absorption maximum $h\nu_{max}$ is evaluated in the context of a thermodynamic cycle.

Soon after, another theory was proposed by Smith and Symons, often called the "confined model."[2, 4-6] In this simple treatment, the modeled CTTS states resemble the ground state of a solvated electron "cavity model." The excited electron is confined in an infinitely deep spherical well. The primary solvent shell surrounding the anion has an adjustable radius, leading to a simple particle in a box picture for the excess electron. The absorption maxima are predicted by

$$h\nu_{max} = E_I + \frac{h^2}{8m_e r_0^2} \qquad (2)$$

Although the Platzman and Franck model predicted CTTS $h\nu_{max}$ values for anions very close to their experimental values, it was incapable of explaining the temperature dependence of $h\nu_{max}$ with available data below 100 °C or the impact of environmental changes on its position. Stein and Treinin overcame this shortcoming by retaining the underlying theory of Platzman and Franck but adopting a different thermodynamic cycle (Fig. 1).[7, 8] An adjustable parameter was introduced to describe the anion cavity radius, $r_0$. This theory is usually referred to as the "diffuse model" for CTTS transitions, which was shown to work well when applied to experimental data available at the time acquired below 100 °C. In the diffuse model approach,

[a] Department of Physical Sciences, Benedictine University, 5700 College Rd., Lisle, IL 60532, USA
[b] Notre Dame Radiation Laboratory, Notre Dame, IN, 46556, USA
* Email: tmarin@ben.edu

Electronic Supplementary Information (ESI) available: [details of any supplementary information available should be included here]. See DOI: 10.1039/x0xx00000x

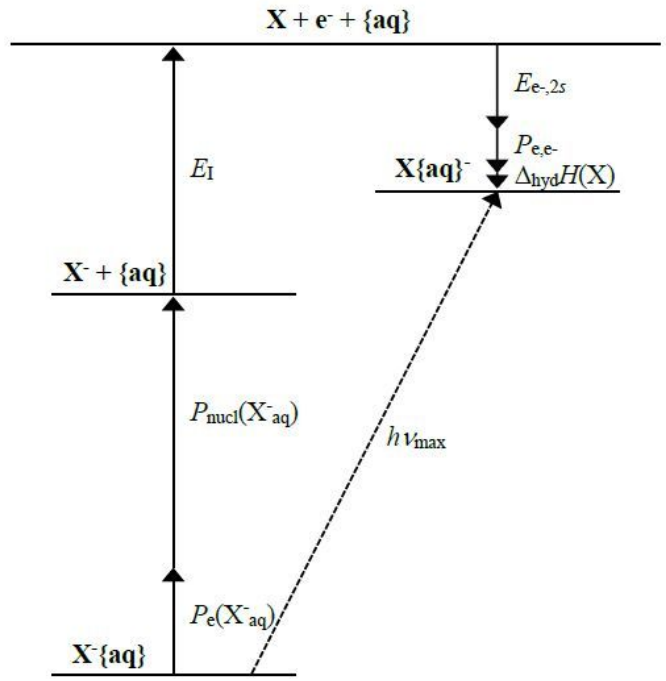


**Figure 1.** Thermodynamic cycle for CTTS transitions, as described by Stein and Treinin.[7, 8] See text for definitions. The magnitudes of each energy contribution are drawn to scale for the $I^-$ absorption.

the aqueous solvent cavity {aq} occupied by the solute anion $X^-$ is preserved throughout the thermodynamic cycle; the cavity remains intact upon the removal of $X^-$ due to the ultrafast electronic processes. The interaction energy of $X^-$ with {aq} and surrounding solvent is accounted for by the sum of $P_e(X^-_{aq})$, the electronic polarization of the solvent caused by the anion, and $P_{nucl}(X^-_{aq})$, the potential energy of the ion due to persistent atomic and dipolar polarization of the solvent.

$$P_e\left(X^-_{aq}\right) = \frac{k_e e^2}{2r_0}\left(1 - \frac{1}{\varepsilon_{op}}\right) \qquad (3)$$

$$P_{nucl}\left(X^-_{aq}\right) = \frac{k_e e^2}{r_0}\left(\frac{1}{\varepsilon_{op}} - \frac{1}{\varepsilon_s}\right) \qquad (4)$$

where $k_e$ is Coulomb's constant, $(4\pi\varepsilon_0)^{-1}$. Upon removal of these energies, a gas-phase anion and the solvent cavity remain, $X^-$ + aq. With addition of ionization energy $E_I$, a gas-phase electron $e^-$ and neutral parent atom X are produced, while the solvent cavity aq still remains intact. The electron is then reinserted in the solvent cavity, and its energy $E_{e^-,2s}$ is equated to that of a relatively diffuse hydrogenic 2*s* orbital electrostatically bound by an effective charge $\left[1/\varepsilon_{op} - 1/\varepsilon_s\right]$ due to the solvent dielectric continuum.

$$E_{e^-,2s} = \frac{2k_e^2\pi^2 m_e e^4}{n^2h^2}\left(\frac{1}{\varepsilon_{op}} - \frac{1}{\varepsilon_s}\right)^2 \qquad (5)$$

Here $m_e$ is the electron mass, $h$ is Planck's constant, and $n$ = 2, per the 2*s* wavefunction. Like $X^-$, the electron also induces a solvent electronic polarization given by

$$P_{e,e^-} = \frac{k_e e^2}{2r_{2s}}\left(1 - \frac{1}{\varepsilon_{op}}\right) \qquad (6)$$

where $r_{2s}$ represents the average radius of the 2*s* wavefunction. Last, the neutral atom X is also inserted into the negatively charged solvent cavity to give $X\{aq\}^-$. Considering the very minor polarization effects for neutral species X, the energy is approximated as the heat of hydration, $\Delta_{hyd}H(X)$. Putting together all these terms for the cycle, the absorption maximum (in Joules) is predicted by

$$h\nu_{max} = \left[P_e\left(X^-_{aq}\right) + P_{nucl}\left(X^-_{aq}\right)\right] + E_I - \left[E_{e^-,2s} + P_{e,e^-} + \Delta_{hyd}H\left(X\right)\right] \qquad (7)$$

Essentially, $r_0$ can be calculated if all other parameters are known, and historically calculated ionic radii were very close to those obtained by analyzing partial molar volumes.

The confined and diffuse models differ most markedly in how the CTTS excited state is constrained. Both essentially use a radius parameter that is sensitive to the applied constraints. Arguably, the superiority of either model has never been demonstrated, whether experimentally or theoretically. Regardless, the confined model suffers from two important defects: 1.) a potential well with extremely steep walls that completely confine the excited-state electron seems less reasonable than the shallow potential well of the diffuse theory, and 2.) the experimental values of $h\nu_{max}$ used to calculate $r_0$ yield values some 2 Å larger than might be realistically expected. Further UV spectroscopic investigations of CTTS bands of aqueous halides and hydroxide occurred throughout the 1970s[9-13], primarily focusing on solvent and temperature dependence and deconvolution of the CTTS bands. However, neither the confined nor diffuse CTTS models were applied in any of these instances. From that time onward, great strides have been made to understand CTTS dynamics, but traditional direct experimental absorption/ transmission investigation of CTTS bands in bulk solution has been minimal.

In the 1990s Sheu and Rossky[14-16] and Staib and Borgis[17, 18] used quantum simulations to probe how the dynamical evolution of the water solvent ultimately led to charge separation from the excited halide. The conclusion was that the detachment is strongly dependent on the local configuration around the ion. This variability should be reflected in a distribution of electron ejection times. Several years later, Bradforth and Jungwirth[19] computed the electronic structure of the CTTS state of aqueous iodide, $I^-$, in dynamic equilibrium with the water solvent. The instantaneous arrangement of the local solvent was found to strongly influence the CTTS wavefunction shape and vertical excitation energy for each excited anion. The three lowest excited states are found to resemble a mixture of 2*s* and 2*p* functions, with a single characteristic node in the radial wavefunction. Voids in the first solvation shell were found to arise due to thermal disorder in liquid water, and their instantaneous locations were found to largely define the orientation of the lowest energy CTTS state. It was further determined that the pre-existing polarization of water molecules produced by ground-state $I^-$ sets up a long-range electrostatic field that binds the CTTS state.[19] The wavefunction could be reproduced using partial charges in place of the water nuclei. Molecular dynamics (MD) simulations with polarizable interaction potentials,[20] quantum mechanics/ molecular mechanics (QMMM), and full-quantum MD simulations[21] showed that the solvent shell surrounding polarizable $I^-$ has an anisotropy resulting from an induced dipole on the anion. These studies clarified that overall the water protons point towards $I^-$, but with a large distribution of solvent cavity configurations.

Extensive efforts have been put forth to observe the early-time dynamics of aqueous CTTS states via ultrafast transient absorption (TA) spectroscopy[22-27] and ultrafast photoemission[28-30] These studies indicated that the electron detaches from $I^-$ in 0.1-0.4 ps, and subsequently relaxation of the host solvent cavity forms a solvated

electron in ~1 ps.[24-27, 29] Femtosecond X-ray absorption spectroscopy at the iodine L-edges detected the birth of the neutral halogen. However the time resolution was insufficient to capture the earliest dynamics.[31] Particularly notable are high-time resolution studies on the CTTS states of sodide ($Na^-$) in tetrahydrofuran (THF) and ether solvents,[23, 32-38] which permitted observation of the ejected electron and the neutral sodium atom. Electrons that photodetached from parent anions produced an equilibrated spectrum within 0.5 ps and showed no pump wavelength dependence. The conclusion was that the electrons are ejected into pre-existing solvent voids.

In addition to studies in bulk phases, halide water clusters have also been intensively studied. How the number of water molecules in a cluster affects CTTS excited states was explored by studying absorption spectra and the relaxation dynamics in small clusters.[19, 24, 39-51] In 1996, Johnson, *et al*. reported that the absorption peaks for $I^-(H_2O)_n$ increased from ~3.5 eV for $n$ = 1 to ~4.4 eV for $n$ = 4, indicating the important collective role of water molecules in determining CTTS excited-state features.[42] Recent MD simulations confirm those findings.[52] Photoelectron spectroscopy studies of Markovich, *et al*. and Kammrath, *et al*. also showed that vertical binding energies (VBEs) for $I^-(H_2O)_n$ clusters increased significantly with $n$ at least up to $n$ = 6. This reportedly provides closure of the first solvation shell. With a further increase in $n$ up to $n$ = 60 the corresponding VBE continued to increase but the increase diminished in magnitude.[40, 41, 45] Relaxation dynamics for CTTS excited states of $I^-(H_2O)_n$ and $I^-(D_2O)_n$ clusters were also examined with time-resolved photoelectron imaging.[44, 45] Neumark, *et al*. demonstrated that the number of photoelectrons yielded from $I^-(H_2O)_4$ decayed faster than those from larger $I^-(H_2O)_n$ clusters, implying that electron autodetachment is the primary decay mechanism for small clusters. It was proposed that the dipole moments of small water clusters are too weak to bind the excited electrons in the solvent reorganization process following electron photoexcitation.

In the current studies, the temperature dependence of CTTS transitions for $Cl^-$, $Br^-$, $I^-$, and $OH^-$ was measured for the first time in high-temperature and subcritical water using ultraviolet absorption spectroscopy. Additional data were acquired for $I^-$ in supercritical water. These new results cover a much broader temperature range than all previously available aqueous CTTS data. With these new data in hand, the traditional models for CTTS absorption can be tested for their applicability over this temperature range. We use the models to extract information on changes to the solvent cavity radius as a function of temperature and ascribe some thermodynamics based on a simple Born model approach, with the free energy of solvation given by

$$\Delta_{\text{solv}}G = -\frac{N_A e^2}{8\pi\varepsilon_0 r_0}\left(1-\frac{1}{\varepsilon_s}\right) \qquad (8)$$

where $N_A$ is Avogadro's number. We discuss these findings in the context of recently acquired knowledge regarding hydrogen bonding in subcritical and supercritical water[53] and mature studies of aqueous ionic radii and solvation thermodynamics.[54-56]

## 2. Experimental

Considering that the $I^-$ CTTS absorption spectrum has a large extinction coefficient $\varepsilon$ at its maxima (> 12,500 $M^{-1}$ $cm^{-1}$ at $\varepsilon_{max}$ at 25 °C) and it is considerably separated in wavelength from the rising edge of the water solvent absorption, a conventional benchtop UV/Vis spectrophotometer can be used to conveniently measure it at low concentrations. Regardless, the low-wavelength side of the spectra are obscured by the onset of the lowest-lying water electronic absorption, which redshifts with increasing temperature.[53, 57] For measurements of the $I^-$ absorption, the experimental setup was a flow system attached to a two-path optical cell that sits directly inside a desktop scanning spectrophotometer. Details of the flow system, optical cell, and temperature and pressure control were previously described.[57] The cell is capable of withstanding high temperatures and pressures up to 400 °C and 300 bar. Spectra were obtained using a 6-mm path length from 25 °C up to 350 °C in increments of 25.0 °C, as well as at 380 °C, with an accuracy of ± 0.2 °C. The experimental pressure was 250 bar for all measurements below the critical temperature, with an accuracy of ± 0.2 bar. At 380 °C, pressure was varied from 190 -270 bar. Table I indicates the exact pressure, temperature, and density conditions used, where the densities are obtained from the water equation of state.[58] The spectrophotometer was continuously purged with dry nitrogen gas to prevent the buildup of ozone generated by the deuterium lamp, which absorbs at 255 nm and interferes in our wavelength range of interest. Deionized water samples were obtained from a 4-cartridge, 18.2-MΩ-cm, Barnstead Nanopure system. Measured organic impurity levels were < 10 ppb after purification. Potassium iodide (Sigma-Aldrich, >99%, CAS Number 7681-11-0) solutions were prepared to a give a room temperature

| Sample | Temperature (°C) | Pressure (bar) | Density (g $cm^{-3}$) |
|---|---|---|---|
| KOH | 25 | 12.5 | 0.998 |
| | 100 | 19.7 | 0.959 |
| | 200 | 30.0 | 0.866 |
| KCl | 25 | 119 | 1.003 |
| | 100 | 119 | 0.964 |
| | 200 | 119 | 0.872 |
| | 300 | 119 | 0.719 |
| KBr | 25 | 119 | 1.003 |
| | 100 | 119 | 0.964 |
| | 200 | 119 | 0.872 |
| | 300 | 119 | 0.719 |
| | 350 | 200 | 0.601 |
| KI | 25 | 250 | 1.008 |
| | 50 | 250 | 0.999 |
| | 75 | 250 | 0.986 |
| | 100 | 250 | 0.970 |
| | 125 | 250 | 0.951 |
| | 150 | 250 | 0.930 |
| | 175 | 250 | 0.907 |
| | 200 | 250 | 0.881 |
| | 225 | 250 | 0.853 |
| | 250 | 250 | 0.821 |
| | 275 | 250 | 0.785 |
| | 300 | 250 | 0.743 |
| | 325 | 250 | 0.692 |
| | 350 | 250 | 0.625 |
| | 380 | 190 | 0.107 |
| | 380 | 230 | 0.209 |
| | 380 | 235 | 0.271 |
| | 380 | 240 | 0.383 |
| | 380 | 250 | 0.451 |
| | 380 | 270 | 0.498 |

**Table I.** Experimental pressure, temperature, and density conditions for all acquired spectra.

concentration of 7.57 × $10^{-5}$ M. Solutions were degassed for ~1 hour with argon gas prior to use and then continuously kept under an argon atmosphere. Spectra were acquired with a wavelength resolution of 1 nm.

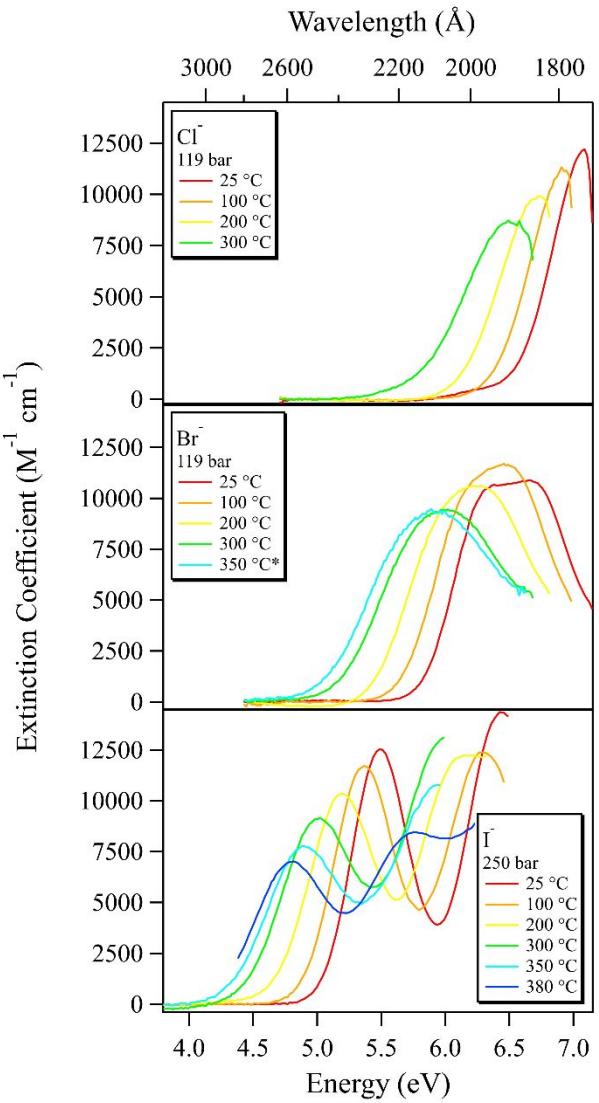


**Figure 2.** CTTS UV absorption spectra for $Cl^-$, $Br^-$, and $I^-$. Pressures and temperatures are as labeled in the figure, except * at 200 bar. Data for selected temperatures are shown for $I^-$.

Due to their occurrence at shorter vacuum ultraviolet wavelengths, absorption spectra for $Cl^-$, $Br^-$, and $OH^-$ were obtained using a synchrotron-based apparatus. The unique nature of the high-sensitivity, high-pressure, high-temperature VUV experiment and technical details regarding the light source and detection, sample cell specifications, sample preparation, temperature/pressure control, and sample flow have been published previously.[53, 59, 60] Despite the fact that $Cl^-$ and $Br^-$ have $\varepsilon_{max}$ values similar to $I^-$, their spectra overlap considerably more with the water solvent absorption, so much higher concentrations are necessary to overwhelm the water background. As with the I- spectra, the blue edge cutoff of the $Cl^-$, $Br^-$, and $OH^-$ absorption is due to the onset of the water absorption, which redshifts with increasing temperature. Potassium chloride (Sigma-Aldrich, >99%, CAS 7447-40-7) and potassium bromide (Sigma-Aldrich, >99%, CAS 7758-02-3) samples were prepared in deionized water as described above to concentrations of 0.025 or 0.250 M, for use with two different path lengths, as described below.

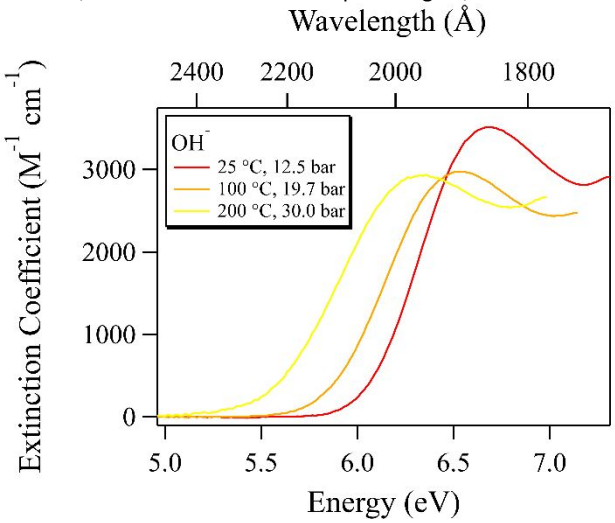


**Figure 3.** CTTS UV absorption spectra for OH-. Pressures and temperatures are as labeled in the figure.

Samples were sparged for at least one hour with helium gas prior to filling the sample cell to remove any residual dissolved gases. Standardized 1.0-N potassium hydroxide solutions (Sigma-Aldrich, CAS 1310-58-3) were used as received. VUV measurements were carried out at the Stainless Steel Seya beam line of the Synchrotron Radiation Center, University of Wisconsin-Madison. The combination of an adjustable path length sample cell, synchrotron light source, and secondary filtering monochromator on the beam line allows for 6 orders of magnitude in light detection dynamic range. Photons were generally counted for 1 s per data point, and photon counts were normalized to fluctuations in the synchrotron beam current in real time during data acquisition. When transmittance was low (< $10^4$ counts $s^{-1}$), photons were counted for up to 20 s per point. Typically, 30 minutes were necessary to acquire an entire spectrum with a wavelength resolution of 5 Å. The beam line monochromator, secondary filtering monochromator, and photon counter were controlled and synchronized through Igor Pro 6.0 run on a notebook PC. The reported spectra are actually composite spectra, compiled from two sample cells with different path lengths to accommodate measuring six orders of magnitude in absorbance/extinction. As for $I^-$, temperature and pressure conditions during measurements were stable within ±0.2 °C and ±0.2 bar, respectively. Measurements were conducted over broader temperature increments, again with values as listed in Table I. Halide CTTS spectra were acquired using gold foil spacers to designate a sample cell path length of 10 □m (for 0.250-M solutions) or 100 □m (for 0.025-M solutions). Spectra for $OH^-$ used a 10-□m path length. Unfortunately, the KOH solutions caused etching of the sapphire windows in the sample cell, so extensive measurements were not possible, and we were unable to exceed a temperature of 200 °C and still acquire quality spectra.

## 3. Results and Discussion

The acquired CTTS spectra for the halides and hydroxide are displayed in Figs. 2 and 3, respectively. The $^2P_{3/2}$, $^2P_{1/2}$ spin-orbit splitting due to the radical excited state is obvious for $I^-$, and for $Br^-$ as well at low temperatures. Maximum extinction coefficients for OH, $Cl^-$, $Br^-$, and the low-energy $^2P_{1/2}$ state for $I^-$ (the high-energy peak is obscured by the water absorption at some temperatures) at each

temperature can be found in Table II. It is clear that with increasing temperature the spectra shift to lower energies and broaden while

| Temperature (°C) | Maximum Extinction Coefficients ($M^{-1}$ $cm^{-1}$) \| at $h\nu_{max}$ (eV) | | | | | | | |
|---|---|---|---|---|---|---|---|---|
| | $Cl^-$ | | $Br^-$ | | $I^-$ | | $OH^-$ | |
| 25 | 12220 | 7.085 | 10890 | 6.666 | 12540 | 5.486 | 3520 | 6.684 |
| 100 | 11350 | 6.907 | 11650 | 6.491 | 11720 | 5.367 | 2970 | 6.525 |
| 200 | 9910 | 6.738 | 10590 | 6.215 | 10350 | 5.188 | 2930 | 6.326 |
| 300 | 8740 | 6.491 | 9450 | 5.990 | 9170 | 5.020 | – | – |
| 350 | – | – | 9370 | 5.904 | 7780 | 4.881 | – | – |
| 380 | – | – | – | – | 7020 | 4.806 | – | – |

**Table II.** Extinction coefficients at energies/wavelengths of maximum absorptivity for CTTS spectra. Note: for $I^-$ only values for the low-energy $^2P_{1/2}$ state are displayed, as the high-energy $^2P_{3/2}$ peak is somewhat obscured by the water absorption at some temperatures.

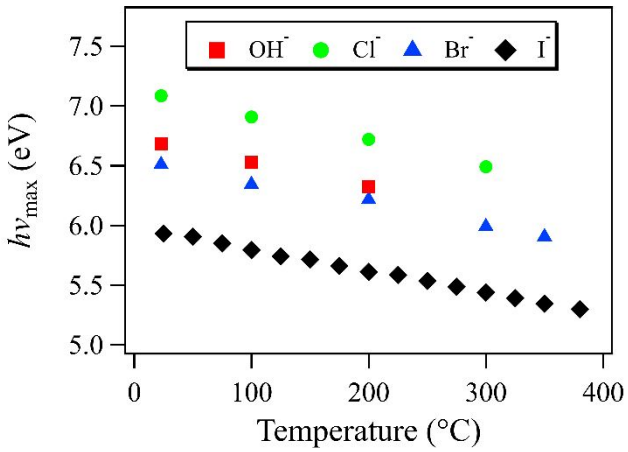


**Figure 4.** Temperature dependence of CTTS absorption maxima, illustrating a linear decrease with increasing temperature.

decreasing in extinction, effectively smearing out the spin-orbit structure for $Br^-$ by 200 °C. The extent of temperature shift in the absorption energy is shown in Fig. 4. Note, considering the spin-orbit structure, we report energy values for $h\nu_{max}$ that correspond to the energy of the band center, not the absolute absorption maximum, so as to capture the average energy of the two spin-orbit states. For $I^-$, this indicates the *minimum* absorptivity between the two peaks. Within experimental limits, the temperature shifts $d(h\nu_{max})/dT$ for all ions are observed to be linear with values as indicated in Table III. We investigated the extent of broadening by focusing on $I^-$ and $Br^-$, as their spectra are least obscured by the water solvent absorption. A two-Gaussian fit reasonably reproduces the spectra at every temperature, and the integral of the fitted function is preserved. Hence, the loss of extinction with increasing temperature is compensated by the extent of broadening, and oscillator strength is preserved. We can only assume the same is true for $Cl^-$ and $OH^-$, as the onset of the water overlaps too greatly with the CTTS absorption to analyze them well. Spectra acquired for iodide at 380 °C showed no energy shift within the limit of our spectral resolution as a function of pressure/density.

The confined and diffuse CTTS models described above allow for prediction of the ionic cavity radius as a function of temperature.

Application of the Stein-Treinin diffuse model[7, 8] gives $r_0$ values for the various anions as shown in the top panel of Fig. 5, where values increase roughly linearly with increasing temperature. Attempts at applying the Smith-Symons confined model[2, 5] resulted in physically unrealistic values for $r_0$ that were over 50% larger than those calculated with the diffuse model, so we did not pursue that model further.

Plugging the calculated ionic radii into Eq. 8 provides the free energy of solvation at each temperature, and these values are shown in the bottom panel of Fig. 5. Seemingly the free energy also scales linearly with increasing temperature, gradually becoming less negative, and implying a weaker extent of solvation at higher temperatures. The linear slope further implies a constant entropy and enthalpy of solvation for each anion, per the standard Gibbs function $G = H - TS$. These values are reported in Table III.

Extinction coefficients and band positions at room temperature have values similar to those previously reported.[1, 9] However, with the exception of $OH^-$, the CTTS energy shift $d(h\nu_{max})/dT$ is significantly greater than that observed in previous work (Table III). Given that previous studies were conducted only below 100 °C, one might consider that there is nonlinearity in the temperature dependence that becomes more obvious over a wider temperature range. However, application of a polynomial fit over our wide temperature range does not significantly improve upon the linear fit. In fact, fitting the data we acquired for $I^-$ in increments of 25 °C still shows a larger slope than that reported in the original studies (Table III). We are uncertain as to why this disagreement exists. Room-temperature values of $r_0$ calculated with the diffuse model exceed values determined by a number of X-ray scattering and thermodynamics experiments and molecular dynamics simulations.[55, 61] For the halides, values are 10-20% too large, and for $OH^-$ the value is over 40% too large. One might question the specific choice of the 2*s* excited state inherent to the diffuse model. In the studies of Bradforth and Jungwirth,[19] all snapshots of the molecular dynamics trajectory examined showed that the CTTS wavefunction maintained a node between the iodide core and frontier lobes. The overall orbital appearance was a mixture of *s*- and *p*-character with a radial node reminiscent to that of a hydrogenic 2*s* wavefunction. To go to the extreme, one can replace the 2*s* hydrogenic wavefunction in the diffuse model with a slightly more compact 2*p* orbital. However, this results in only a ~2% reduction in $r_0$. Within the diffuse model, it is undoubtedly the ionic polarization terms in Eqs. 3 and 4 that

| anion | $d(h\nu_{max})/dT$ (meV $K^{-1}$) | | $\Delta_{solv}S$ (kJ $mol^{-1}K^{-1}$) | | $\Delta_{solv}H$ (kJ $mol^{-1}$) | |
|---|---|---|---|---|---|---|
| | exp | lit | exp | lit[d] | exp | lit[e] |
| $OH^-$ | -2.04 | -2.09[a] | -0.153 | -0.161 | -476 | -520 |
| $Cl^-$ | -2.11 | -1.40[b] | -0.149 | -0.075 | -364 | -367 |
| $Br^-$ | -1.82 | -1.43[c] | -0.133 | -0.059 | -342 | -336 |
| $I^-$ | -1.81 | -1.43[c] | -0.132 | -0.036 | -329 | -291 |

ARTICLE

**Table III.** Fitted slope of experimental band center energies and thermodynamic parameters for solvation extracted from Born analysis of experimental data (exp), and literature (lit) comparison. *a*, *b*, *c*, *d*, and *e* correspond to references 9, 10, 1, 56, and 54, respectively.

contribute most significantly to the overall thermodynamic cycle. Considering that a basic Landau theory of continuous medium is used as a first approximation to arrive at these terms, the results of the model can only be taken at face value and must be interpreted judiciously. We do note that the overall trend in the calculated radii is sensible, that is $OH^- < Cl^- < Br^- < I^-$.

Perhaps the most shocking revelation is that $h\nu_{max}$, $r_0$, and $\Delta_{solv}G$ all show basically linear dependence on temperature. Furthermore, the slopes of each are nearly the same, irrespective of the anion being examined. We turn to the diffuse model to consider how this might be possible. $r_0$ depends significantly on the properties of water dielectric medium, as dictated by Eqs. 3-7. Per the hydrogenic orbitals used in the diffuse model, the orbital energy varies as

$$E_n = -\frac{13.6 Z_{eff}^{\ 2}}{n^2} \qquad (9)$$

For $n$ = 2, this gives energies ranging from 1.05-1.34 eV over the range 25-350 °C, corresponding to wavelengths of 1.18-0.93 $\mu$m, per the Planck-Einstein relationship. The square of the refractive index at each of these wavelengths at their corresponding temperatures, as taken from Harvey, *et al*,[62] was used to generate $\varepsilon_{op}$. Values for $\varepsilon_s$ were taken from Uematsu and Frank.[63] The temperature dependence of both dielectric constants is shown in Fig. 6. Examining the figure, one might envision that the nonlinear trends with increasing temperature would have a nonlinear effect on $r_0$, yet the observed trend in $r_0$ with increasing temperature is linear. To investigate, the impact of $\varepsilon_s$ and $\varepsilon_{op}$ on $r_0$ in Eq. 7 was isolated by holding $h\nu_{max}$ constant at its room temperature value. The result is shown by the green curve in Fig. 7, where the value for $Br^-$ at 25 °C was used for $h\nu_{max}$. This picture suggests that the ionic cavity radius should decrease slightly with increasing temperature due to changes in the water dielectric properties. The change is small, only a 2.5% decrease by 350 °C, but a concave down curvature in the temperature dependence of $r_0$ is obvious. Similarly, $\varepsilon_s$ and $\varepsilon_{op}$ were held constant at their 25 °C values while letting $h\nu_{max}$ assume the experimentally measured values for $Br^-$. This produces the blue curve in Fig. 7, which has a slight upward concavity. Allowing all parameters to work in concert produces the red curve. The function is linear within limits of experimental precision. Coincidentally, the temperature dependences of $r_0$ and $\varepsilon_s$ work in a similar cooperative fashion in Eq. 8 to give $\Delta_{solv}G$ a near-linear temperature dependence.

We turn to our recent spectroscopic studies of subcritical and supercritical water[53] to address the temperature dependence of $h\nu_{max}$. In those studies, the lowest-lying electronic absorption in bulk water shows a gradual redshift with increasing temperature, with a slope $dE/dT$ = -2.03 meV °C$^{-1}$. This energy shift was discussed in terms of a breakdown in hydrogen bonding with increasing temperature

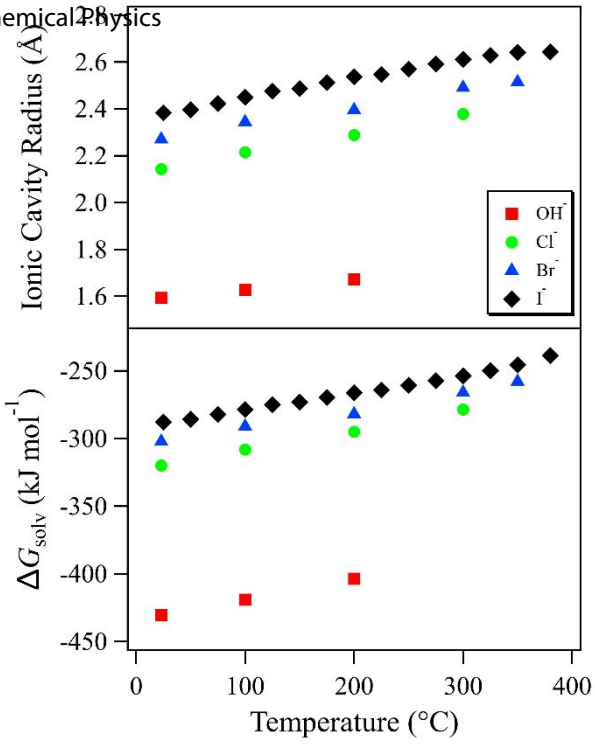


**Figure 5. (top)** Ionic cavity radii as a function of temperature, as calculated from the diffuse model for CTTS absorptions.[7, 8] **(bottom)** Free energy of solvation as a function of temperature, as calculation from the Born equation.

and its effects on the ground-state and excited-state energies. It is surprising to discover that this energy shift is almost identical to $d(h\nu_{max})/dT$ values listed in Table III for the CTTS absorptions. We propose that the extent of electrostatic interactions between the ions and surrounding water solvent may follow a trend no different than the hydrogen bonding interactions between the water molecules themselves. In short, increasing thermal energy disrupts the solvent-solvent and solvent-solute interactions alike, and possibly all that is being witnessed is an increase in the ground-state energy due to a decreased level of hydration. This actually may give us insight into the nature of the water shift itself, suggesting that changes to the ground-state are primarily responsible for the energy shift.

Spectroscopic studies of $I^-(H_2O)_n$ clusters qualitatively show similar behavior – the presence of solvating water molecules shifts the absorption $I^-$ CTTS absorption to higher energy all the way up to $n$ = 60.[40-42] Comparing to these data acquired at a temperature near 70 K to our $I^-$ data in supercritical water may not be a fair comparison, but taken at face value the 4.81-eV absorption that we observe for $I^-$ in supercritical water at 380 °C at all pressures/densities indicates approximately 5 water molecules associated with the anion. Considering that the equilibrium properties of supercritical water[64-66] dictate domination by water monomers and minority contributions from dimers and trimers under all these conditions, we propose that $I^-$ is capable of binding more water molecules into a cluster than persist in supercritical water clusters alone. If the size of this cluster grows with increasing density, the corresponding lack of spectral shift suggests that the ion has already achieved dielectric saturation at the lowest density measured, 0.107 g cm$^{-3}$, an effect

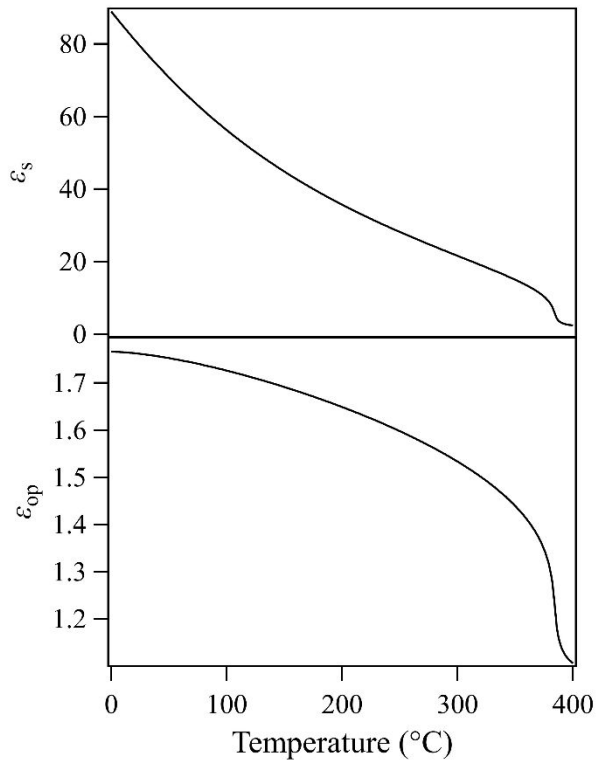


**Figure 6.** Temperature dependence of static $\varepsilon_s$ and optical $\varepsilon_{op}$ dielectric constants for water.[62, 63] Functions shown are for a 250-bar isobar and the refractive index at 1.07 $\mu$m, the wavelength corresponding to the average 2*s* orbital energies over the range 25-350 °C.

not encountered with increasing cluster size in previous work.[40-42] This may not be surprising, as recent studies of aqueous ion solvation have shown that dielectric saturation can be reached or nearly reached at elevated temperatures and pressures near the critical point for ions that do not achieve such saturation under ambient conditions.[67] This includes all the ions examined in this study. In support of our conclusion, we note that molecular dynamics studies of chloride ion hydration in supercritical water indicate that the ion hydration number slowly decreases with density, but confirm the presence of at least 6 water molecules per cluster over our entire density range.[68]

Without question, application of a simple Born continuum solvation model is flawed in that it does not account for the different orientations of water molecules in the first hydration shells. However, it does give insight into several items. First, the free energy of solvation steadily becomes less negative, decreasing in magnitude with increasing temperature. Considering that the literature values for the solvation entropy[56] are negative in value, this is the expected result. However, per the values in Table III the slope $d(\Delta_{solv}G)/dT$ is too large for all species with the exception of $OH^-$. This is a surprise in that the Born equation is expected to fail most considerably for this particular ion. Second, the solvation energy remains enthalpy dominated over the entire temperature range studied. As suggested by theories of hydration,[69] the negative entropy change associated with the ion-water interaction is largely cancelled by a positive entropy change encountered by the water solvent reorganization.

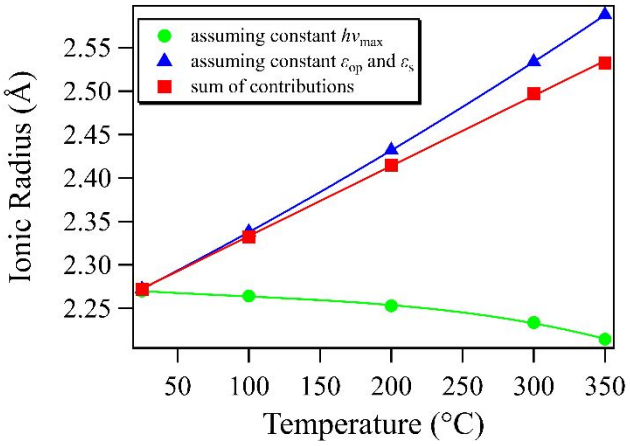


**Figure 7.** Dependence of ionic cavity radius $r_0$ on water dielectric constants $\varepsilon_s$ and $\varepsilon_{op}$ (green circles) while holding $h\nu_{max}$ constant at the value for $Br^-$ at 25 °C. This is compared to the dependence on $h\nu_{max}$ (blue triangles) while holding $\varepsilon_s$ and $\varepsilon_{op}$ constant at their values at 25 °C. Their red squares show their combined effect. The points correspond to experimental temperatures. Curves are drawn merely to guide the eye.

This results in an overall small entropy change whose value is nearly irrespective of the ion and an overall Gibbs free energy change that is highly enthalpy driven due to simple electrostatics of the anion-water interaction; the entropy component is thus difficult to probe and the reported values in Table III must be taken with discretion. Conversely, the enthalpy values calculated based on the simple Born model all lie within 15% of literature values.[54]

Given the high concentrations used in these studies and considerable decrease in $\varepsilon_s$ with increasing temperature, as shown in Fig. 6, the possibility of ion pairing and even precipitation must be considered. While careful temperature-dependent conductivity studies of KCl and KOH have been performed,[70, 71] to our knowledge specific studies of KBr and KI do not exist. The reported association constants indicate that for our experimental conditions, significant ion pairing must exist. This effect will of course be most important for our highest concentration solutions. For 1.0-M KOH at 200 °C, the extent of dissociation is expected to be less than 50%. For 0.25-M KCl at 300 °C, it is on the order of 40%. Despite these values the ion pairs must remain solvated, as in our experiments there was no evidence of precipitation. The sample cell remained transparent and the spectra showed no evidence of Rayleigh scattering. As already mentioned, oscillator strength is preserved at least for $I^-$ and $Br^-$ with increasing temperature, remarkably showing no indication that there is loss of CTTS intensity due to ion pair formation. The fact that $Cl^-$ and $OH^-$ show a linear temperature dependence for $h\nu_{max}$, just like $Br^-$ and $I^-$ suggests similar behavior.

Certainly, the presence of an opposing charge adjacent to the anion associated with the CTTS absorption must significantly perturb the anion polarization and that of the solvent, greatly affecting the orbitals involved in the CTTS transition. We have not accounted for these effects, nor does the diffuse CTTS model incorporate them. Regardless of any perturbation, history shows studies of CTTS transitions of ion pairs in nonpolar solvents, as well as in the solid phase and in the gas phase. Blandamer and Fox (and references therein) again have provided a thorough overview.[1] A major point is

that in any pure solvent two distinct CTTS bands identifiable with ion pairs and separated ions have never been observed. For CTTS transitions in nonpolar solvents where ion pairs necessarily form, the value of $h\nu_{max}$ does depend on the associated cation, as it perturbs the transition as mentioned above. In a given solvent, $h\nu_{max}$ generally increases with an decrease in cation size.[72] This cation dependence of $h\nu_{max}$ is understandable in terms of increased electrostatic stabilization of the ion pair with decreased distance between the individual ion charge centers. A decrease in the interionic distance leads to greater CTTS ground-state stabilization, shifting $h\nu_{max}$ to higher energies. If just a small amount of polar solvent is added to these systems, the spectrum slightly blueshifts, showing a preferential solvation by the more polar component, but there is no abrupt shift in the spectrum.[73] At these low concentrations of added polar solvent, $h\nu_{max}$ depends on the nature of the cation until reaching a certain composition, beyond which it become independent of the cation. However, a smooth and gradual blueshift in the CTTS band continues as more polar solvent is added, while the CTTS transition due to the ion pair must smoothly transform into the normal CTTS transition of the free ions. For cation-iodide pairs that are known not to be completely associated in solution, there is a remarkable coincidence of the cation and solvent dependence of $h\nu_{max}$ for both free and associated iodide.[74] The gradual band shift with added polar solvents shows that the difference in energies between free and associated iodide is small. In removing the solvent altogether, the CTTS absorption feature remains for both gas-phase and solid-phase ion pairs. Moreover, $d(h\nu_{max})/dT$ for iodide crystals is similar to that found for aqueous iodide. With our current data, even though ion pairs could contribute significantly to the measured spectra, we cannot deconvolute their contribution from that of the separated solvated ions. A thorough systematic investigation of these ion pairing effects at elevated temperatures as a function of salt concentration and cation identity will be a topic of our future studies.

Given all of the observations from the current and previous studies, a big question remains: why should the simple diffuse model based on a continuum solvent polarization successfully model the nature of the CTTS absorption over the entire range of conditions studied? The most general descriptions of aqueous ion solvation suggest an inner solvation shell with water molecules oriented to energetically accommodate the ion presence, and a gradual transition to outlying solvation shells geometrically oriented in such a fashion as to constitute the polarization of the water dielectric continuum. However, the extent of the inner shell structure highly depends on both the charge of the ion as well as its size. For the monovalent ions studied in these experiments, the extent of the inner-shell structure is known to be less than that of small alkali cations, for example, yet somewhat well-defined ion hydration shells are observed in scattering experiments.[67, 75-77] However the weak local electric field generated by these ions is simply insufficient to saturate the water dipoles in their vicinity. If this is truly the case, then perhaps for subcritical water even the inner hydration shell can be treated to a first approximation as part of the water continuum, and the diffuse model is valid in this regard. This notion likely breaks down above the critical temperature, though potential ion pairing effects may coincidentally align the CTTS band shift with a subcritical extrapolation of $d(h\nu_{max})/dT$.

## Conclusions

The temperature dependence of VUV CTTS absorption spectra of aqueous $Cl^-$, $Br^-$, $I^-$, and $OH^-$ was measured up to 380 °C in subcritical and supercritical water. The absorption spectra broaden and redshift with increasing temperature, extending previous measurements below 100 °C.[1] The shifts in the spectral peak with respect to temperature $d(h\nu_{max})/dT$ are observed to be linear in nature for all ions studied. With these data in hand, we applied historic models for CTTS transitions that have gone virtually untested for nearly 60 years. The Stein-Treinin diffuse model[7, 8] was applied to all systems to ascertain changes to the anion cavity radius $r_0$ with increasing temperature, giving values that increase roughly linearly with increasing temperature despite the nonlinear temperature dependence of the water dielectric properties inherent to the model. Furthermore, it produces realistic $r_0$ values and trends as a function of both temperature and chosen anion – a surprising result for this relatively simple solvent continuum model. We have discussed the success of this model considering the known lack of structure within the hydration shells of the studied anions at elevated temperatures.[75, 76] Applying a simple Born solvation model shows that the free energy of solvation also scales linearly with increasing temperature, gradually becoming less negative in value, which indicates a weaker extent of solvation at higher temperatures. The linear slope implies a constant entropy and enthalpy of solvation for each anion, regardless of temperature. The lowest-lying electronic absorption in water[53] shows a peak energy shift with increasing temperature that is almost identical to the $d(h\nu_{max})/dT$ values for the CTTS absorptions. Seemingly, increasing temperature disrupts interactions in the same fashion, whether solvent-solvent or solvent-solute. The CTTS absorptions and water absorptions alike may simply be showing an increase in the ground-state energy due to a decreased extent of hydration. The 4.81-eV peak energy for the $I^-$ CTTS absorption in supercritical water at 380 °C is unvarying at all experimental pressures/densities. Comparison to previous studies of $I^-$ in water clusters suggests association with approximately 5 water molecules. The implications are that $I^-$ is capable energetically of binding more water molecules into a cluster than supercritical water can on its own, and that dielectric saturation exists at all the supercritical pressures/densities measured. We have additionally discussed how ion pairing effects must certainly contribute to the CTTS absorption energy, and a thorough study of these effects will be a focus of future work.

## Conflicts of interest

There are no conflicts to declare.

## Acknowledgements

This work is based largely upon research conducted at the Synchrotron Radiation Center, University of Wisconsin-Madison, which was supported by the National Science Foundation (NSF) under Award DMR-0537588. The help of the SRC staff is greatly appreciated. We also thank the Nanofabrication Facility staff and machine shop staff of the Physics Department at the University of Notre Dame. We thank K. Takahashi for the sample used cell in $I^-$ measurements. The research described herein was supported by the Division of Chemical Sciences, Geosciences, and Biosciences, Basic Energy Sciences, Office of Science, United States Department of Energy, through grant DE-FC02-04ER15533. This is contribution

 

number NDRL-5225 from the Notre Dame Radiation Laboratory. T. W. Marin was funded by Research Corporation for Science Advancement CCSA Award 7693, National Science Foundation-RUI Award 0809467, and the Benedictine University College of Science.

## References

**REFERENCES**

1. M. J. Blandamer and M. F. Fox, *Chem. Rev.*, 1970, **70**, 59-93.
2. M. Smith and M. C. R. Symons, *Trans. Faraday Society*, 1958, **54**, 338-345.
3. R. Platzman and J. Franck, *Z. Phys.*, 1954, **138**, 411-431.
4. M. Smith and M. C. R. Symons, *Discuss. Faraday Soc.*, 1957, **24**, 206-215.
5. M. Smith and M. C. R. Symons, *Trans. Faraday Society*, 1958, **54**, 346-352.
6. T. R. Griffiths and M. C. R. Symons, *Trans. Faraday Society*, 1960, **56**, 1125-1136.
7. G. Stein and A. Treinin, *Trans. Faraday Society*, 1959, **55**, 1086-1090.
8. G. Stein and A. Treinin, *Trans. Faraday Society*, 1959, **55**, 1091-1099.
9. M. Fox, R. McIntyre and E. Hayon, *Farad. Discuss.*, 1977, **64**, 167-172.
10. M. F. Fox, B. E. Barker and E. Hayon, *J. Chem. Soc. Faraday Trans. 1*, 1978, **74**, 1776-1785.
11. M. F. Fox and E. Hayon, *Chem. Phys. Lett.*, 1972, **14**, 442-444.
12. M. F. Fox and E. Hayon, *Chem. Phys. Lett.*, 1974, **25**, 511-514.
13. M. F. Fox and E. Hayon, *J. Chem. Soc. Faraday Trans. 1*, 1977, **73**, 1003-1016.
14. W. S. Sheu and P. J. Rossky, *J. Am. Chem. Soc.*, 1993, **115**, 7729-7735.
15. W.-S. Sheu and P. J. Rossky, *Chem. Phys. Lett.*, 1993, **202**, 186-190.
16. W.-S. Sheu and P. J. Rossky, *J. Phys. Chem.*, 1996, **100**, 1295-1302.
17. A. Staib and D. Borgis, *J. Chem. Phys.*, 1995, **103**, 2642-2655.
18. A. Staib and D. Borgis, *J. Chem. Phys.*, 1996, **104**, 9027-9039.
19. S. E. Bradforth and P. Jungwirth, *J. Phys. Chem. A*, 2002, **106**, 1286-1298.
20. C. D. Wick and S. S. Xantheas, *J. Phys. Chem. B*, 2009, **113**, 4141-4146.
21. V. T. Pham, I. Tavernelli, C. J. Milne, R. M. van der Veen, P. D'Angelo, C. Bressler and M. Chergui, *Chem. Phys.*, 2010, **371**, 24-29.
22. A. E. Bragg, M. C. Cavanagh and B. J. Schwartz, *Science*, 2008, **321**, 1817-1822.
23. A. E. Bragg and B. J. Schwartz, *J. Phys. Chem. B*, 2008, **112**, 483-494.
24. X. Chen and S. E. Bradforth, *Annu. Rev. Phys. Chem.*, 2008, **59**, 203-231.
25. H. Iglev, A. Trifonov, A. Thaller, I. Buchvarov, T. Fiebig and A. Laubereau, *Chem. Phys. Lett.*, 2005, **403**, 198-204.
26. J. A. Kloepfer, V. H. Vilchiz, V. A. Lenchenkov and S. E. Bradforth, *Chem. Phys. Lett.*, 1998, **298**, 120-128.
27. A. C. Moskun, S. E. Bradforth, J. Thøgersen and S. Keiding, *J. Phys. Chem. A*, 2006, **110**, 10947-10955.
28. A. Lübcke, F. Buchner, N. Heine, I. V. Hertel and T. Schultz, *PCCP*, 2010, **12**, 14629-14634.
29. Y. Tang, Y.-i. Suzuki, H. Shen, K. Sekiguchi, N. Kurahashi, K. Nishizawa, P. Zuo and T. Suzuki, *Chem. Phys. Lett.*, 2010, **494**, 111-116.
30. F. Messina, O. Braem, A. Cannizzo and M. Chergui, *Nat. Commun.*, 2013, **4**.
31. V.-T. Pham, T. J. Penfold, R. M. van der Veen, F. Lima, A. El Nahhas, S. L. Johnson, P. Beaud, R. Abela, C. Bressler, I. Tavernelli, C. J. Milne and M. Chergui, *J. Am. Chem. Soc.*, 2011, **133**, 12740-12748.
32. O. Shoshana, J. L. Perez Lustres, N. P. Ernsting and S. Ruhman, *PCCP*, 2006, **8**, 2599-2609.
33. O. Shoshanim and S. Ruhman, *J. Chem. Phys.*, 2008, **129**, 044502.
34. A. E. Bragg, G. U. Kanu and B. J. Schwartz, *J. Phys. Chem. Lett.*, 2011, **2**, 2797-2804.
35. A. E. Bragg and B. J. Schwartz, *J. Phys. Chem. A*, 2008, **112**, 3530-3543.
36. W. J. Glover, R. E. Larsen and B. J. Schwartz, *J. Chem. Phys.*, 2008, **129**, 164505.
37. W. J. Glover, R. E. Larsen and B. J. Schwartz, *J. Chem. Phys.*, 2010, **132**, 144101.
38. M. C. Larsen and B. J. Schwartz, *J. Chem. Phys.*, 2009, **131**, 154506.
39. N. Galamba, R. A. Mata and B. J. C. Cabral, *J. Phys. Chem. A*, 2009, **113**, 14684-14690.
40. G. Markovich, R. Giniger, M. Levin and O. Cheshnovsky, *J. Chem. Phys.*, 1991, **95**, 9416-9419.
41. G. Markovich, S. Pollack, R. Giniger and O. Cheshnovsky, *J. Chem. Phys.*, 1994, **101**, 9344-9353.
42. D. Serxner, C. E. H. Dessent and M. A. Johnson, *J. Chem. Phys.*, 1996, **105**, 7231-7234.
43. P. Ayotte, C. G. Bailey, G. H. Weddle and M. A. Johnson, *J. Phys. Chem. A*, 1998, **102**, 3067-3071.
44. L. Lehr, M. T. Zanni, C. Frischkorn, R. Weinkauf and D. M. Neumark, *Science*, 1999, **284**, 635-638.
45. A. Kammrath, J. R. R. Verlet, A. E. Bragg, G. B. Griffin and D. M. Neumark, *J. Phys. Chem. A*, 2005, **109**, 11475-11483.
46. D. E. Szpunar, K. E. Kautzman, A. E. Faulhaber and D. M. Neumark, *J. Chem. Phys.*, 2006, **124**, 054318.
47. O. T. Ehrler and D. M. Neumark, *Acc. Chem. Res.*, 2009, **42**, 769-777.
48. A. K. Pathak, *Chem. Phys. Lett.*, 2011, **512**, 129-132.
49. C. C. Mak and G. H. Peslherbe, *Mol. Simulat.*, 2015, **41**, 156-167.
50. L. Turi and P. J. Rossky, *Chem. Rev.*, 2012, **112**, 5641-5674.
51. R. M. Young and D. M. Neumark, *Chem. Rev.*, 2012, **112**, 5553-5577.
52. M.-F. Chiou and W.-S. Sheu, *Int. J. Quantum Chem.*, 2017, **117**, e25404-n/a.
53. T. W. Marin, I. Janik, D. M. Bartels and D. M. Chipman, *Nat. Commun.*, 2017, **8**, 15435.
54. Y. Marcus, *J. Chem. Soc. Faraday Trans. 1*, 1987, **83**, 339-349.
55. Y. Marcus, *J. Chem. Phys.* 2012, **137**, 154501.
56. Y. Marcus and A. Loewenschuss, *Annual Reports Section "C" (Physical Chemistry)*, 1984, **81**, 81-135.
57. T. W. Marin, K. Takahashi and D. M. Bartels, *J. Chem. Phys.*, 2006, **125**.

58. W. Wagner and A. Pruss, *J. Phys. Chem. Ref. Data*, 2002, **31**, 387-535.
59. I. Janik and T. W. Marin, *Nucl. Instrum. Meth. A*, 2013, **698**, 44-48.
60. I. Janik and T. W. Marin, *Rev. Sci. Instrum.*, 2015, **86**.
61. Y. Marcus, *Chem. Rev.*, 1988, **88**, 1475-1498.
62. A. H. Harvey, J. S. Gallagher and J. Sengers, *J. Phys. Chem. Ref. Data*, 1998, **27**, 761-774.
63. M. Uematsu and E. U. Frank, *J. Phys. Chem. Ref. Data*, 1980, **9**, 1291-1306.
64. T. A. Odintsova and M. Y. Tretyakov, *J. Quant. Spectros. Radiat. Transfer*, 2013, **120**, 134-137.
65. M. Y. Tretyakov and D. S. Makarov, *J. Chem. Phys.*, 2011, **134**, 084306.
66. M. Y. Tretyakov, E. A. Serov and T. A. Odintsova, *Radiophys. Quantum Electron.*, 2012, **54**, 700-716.
67. I. Danielewicz-Ferchmin, E. M. Banachowicz and A. R. Ferchmin, *J. Mol. Liq.*, 2013, **187**, 157-164.
68. M. Kubo, R. M. Levy, P. J. Rossky, N. Matubayasi and M. Nakahara, *J. Phys. Chem. B*, 2002, **106**, 3979-3986.
69. D. Ben-Amotz and R. Underwood, *Acc. Chem. Res.*, 2008, **41**, 957-967.
70. P. C. Ho, H. Bianchi, D. A. Palmer and R. H. Wood, *J. Solution Chem.*, 2000, **29**, 217-235.
71. P. C. Ho, D. A. Palmer and R. H. Wood, *J. Phys. Chem. B*, 2000, **104**, 12084-12089.
72. M. J. Blandamer, T. E. Gough and M. C. R. Symons, *Trans. Faraday Society*, 1966, **62**, 286-295.
73. M. J. Blandamer, T. E. Gough and M. C. R. Symons, *Trans. Faraday Society*, 1966, **62**, 296-300.
74. J. H. Beard and P. H. Plesch, *J. Chem. Soc. (Resumed)*, 1964, DOI: 10.1039/JR9640004879, 4879-4887.
75. I. Howell, G. W. Neilson and P. Chieux, *J. Mol. Struct.*, 1991, **250**, 281-289.
76. M. Magini, G. Licheri, G. Paschina, G. Piccaluga and G. Pinna, *X-Ray Diffraction of Ions in Aqueous Solutions: Hydration and Complex Formation*, CRC Press, Boca Raton, FL, 1988.
77. J. L. Fulton, G. K. Schenter, M. D. Baer, C. J. Mundy, L. X. Dang and M. Balasubramanian, *J. Phys. Chem. B*, 2010, **114**, 12926-12937.

Exploring charge-transfer-to-solvent excitation of aqueous halide anions by vacuum ultraviolet spectroscopy – new insights up to 380 °C.

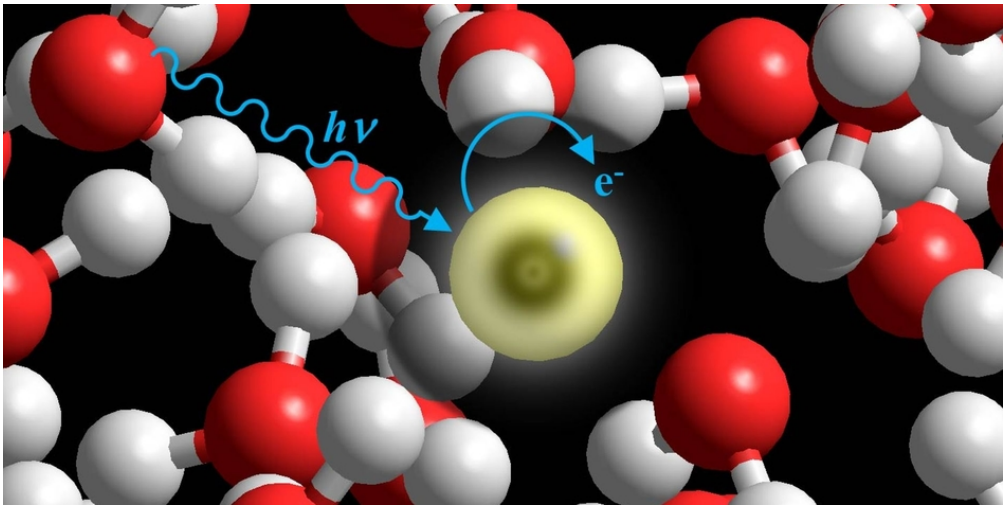


80x40mm (300 x 300 DPI)